Magnetic uniaxial wire medium

Tiago A. Morgado,[1,*] João T. Costa,[2] and Mário G. Silveirinha[1,†]
[1]*Department of Electrical Engineering, Instituto de Telecomunicações, University of Coimbra, 3030 Coimbra, Portugal*
[2]*CST AG, Bad Nauheimer Strasse 19, 64289 Darmstadt, Germany*
(Received 12 September 2015; revised manuscript received 7 January 2016; published 1 February 2016)

It is shown that a racemic array of helical-shaped metallic wires may have a dual electromagnetic response, such that for arbitrarily large wavelengths it concurrently supports two modes with hyperbolic- and elliptical-type dispersions. Importantly, one of the eigenwaves is nearly dispersionless and sees the metamaterial as a medium with extreme magnetic anisotropy. The metamaterial may thus behave as the magnetic analog of the conventional wire medium formed by a set of parallel straight metallic wires. It is demonstrated that the magnetic wire medium enables channeling the subwavelength details of transverse electric (TE) polarized waves.

DOI: 10.1103/PhysRevB.93.075102

I. INTRODUCTION

Since the pioneering works of Abbe [1] and Lord Rayleigh [2], it has been known that the resolution of conventional imaging devices is restricted by the wavelength of light—"the diffraction limit." According to these old studies, features smaller than approximately a half-wavelength of light are invariably absent from the image created by conventional optical lenses. This limitation results from the inability of typical lenses to interact with the fields of spatial harmonics with very high spatial frequencies, which are locked in the near-field spectrum of an optical source. Different from the far-field spectrum, which is radiated away from the source and hence can be captured by common lenses, the near field has an inherent evanescent-wave character that causes its exponential decay.

During the last decade, numerous approaches and technologies were proposed to manipulate the near field and enable imaging beyond the diffraction limit [3–20]. One of the most effective mechanisms relies on the transformation of the entire source spatial spectrum (including evanescent harmonics) into propagating waves at the input interface of a specially designed slab and on its subsequent transport to the output interface. Such a mechanism is designated by "canalization regime" [15–21], and becomes possible if the designed material slab has flat isofrequency contours [15–17,20]. Arrays of parallel metallic wires have been widely used to implement the canalization regime from microwaves to infrared frequencies [16,18–20]. In Refs. [16–20] it was demonstrated that such "wire medium lenses" are able to manipulate and canalize a complex near-field distribution with subwavelength resolution (at least five times superior to that obtained with conventional lenses). However, the wire medium lens is polarization sensitive and only enables near-field imaging of transverse magnetic (TM) polarized waves (magnetic field is parallel to the interface). In other words, the standard wire medium lens (with wires perpendicular to the interface) is completely transparent to transverse electric (TE) polarized waves (electric field parallel to the interface). To overcome this limitation, we suggested in Ref. [22] a post-processing strategy to fully restore the near field radiated by a source with arbitrary polarization using arrays of parallel straight wires. The robustness of this approach was experimentally verified in Ref. [23]. However, such a solution can only be used when the field radiated by the relevant source is stationary in time and requires three independent acquisitions of the near field.

Having a similar channeling effect for TE polarized waves would require using "magnetic wires" [ideally "perfectly magnetic conducting" (PMC) wires] rather than metallic wires. However, a PMC material is mainly a theoretical abstraction because it does not exist in nature. Nevertheless, one may envision that magnetic wires may be implemented relying on the exotic electromagnetic responses provided by metamaterials.

A configuration that partially mimics the magnetic wires is the "Swiss rolls" array [4,5]. This structure consists of a set of cylindrical inclusions, with each element comprising a conducting sheet wound on a central mandrel, so that the cross section is a spiral. It was shown in [4] that at the resonant frequency, the Swiss rolls may be used to transfer an input magnetic near-field distribution to the output interface with a spatial resolution limited by the roll diameter. These Swiss rolls-based lenses are effective at MHz frequencies [4,5]. However, due to fabrication constraints, it seems very difficult to design these structures to operate at higher frequencies (namely, at microwave and optical frequencies). In a slightly different context, a related metamaterial structure with a highly anisotropic magnetic permeability was used to transfer static magnetic fields to arbitrarily long distances [24].

In this work we suggest an alternative way to emulate the response of PMC wires that can be easily scaled to operate in the microwave frequency regime and possibly at higher frequencies. The idea is to use helical-shaped metallic wires which for relatively large radii may enable a strong magnetic response. Specifically, we consider a metamaterial formed by a racemic array of helical-shaped metallic wires with two helices with opposite handedness per unit cell. Notably, it is demonstrated that due to spatial dispersion effects such a metamaterial has a dual electromagnetic response, so that it concurrently supports two extraordinary TE waves with hyperbolic and elliptical-type dispersions. Moreover, one of the eigenmodes has a phase velocity along the axial direction nearly independent of the transverse wave vector, which is analogous to what happens in the standard wire medium

*tiago.morgado@co.it.pt
†Corresponding author: mario.silveirinha@co.it.pt

 ©2016 American Physical Society

(formed by straight metallic wires) under TM excitation [15–17,20]. Therefore, the helical-shaped wire medium—designated as *magnetic wire medium*—may behave as the magnetic dual of the standard wire medium.

This paper is organized as follows. In Sec. II the geometry of the metamaterial is described and a nonlocal homogenization model that characterizes its electromagnetic response is proposed. In Sec. III the plane wave scattering by a metamaterial slab is studied using both homogenization theory and full-wave simulations. In Sec. IV it is demonstrated that the proposed metamaterial lens may enable the transport of the subwavelength details of TE polarized waves. Finally, the conclusions are drawn in Sec. V.

II. HOMOGENIZATION MODEL

The metamaterial considered here consists of a racemic array of metallic [ideally perfect electric conductors (PECs)] helical-shaped wires oriented along the z direction (Fig. 1). The unit cell is rectangular (with period $a_x = 2a$ along the x direction and a along the y direction) and includes two helical-shaped wires with opposite handedness, i.e., one right-handed helix and one left-handed helix. Thus, since the structure has a center of symmetry, the electromagnetic response of the metamaterial is nonbianisotropic. Related metamaterial structures have been considered previously in different contexts [25–31], namely in the realization of circular polarizers and wave plates [26,27], and in focusing based on a negative refraction [31].

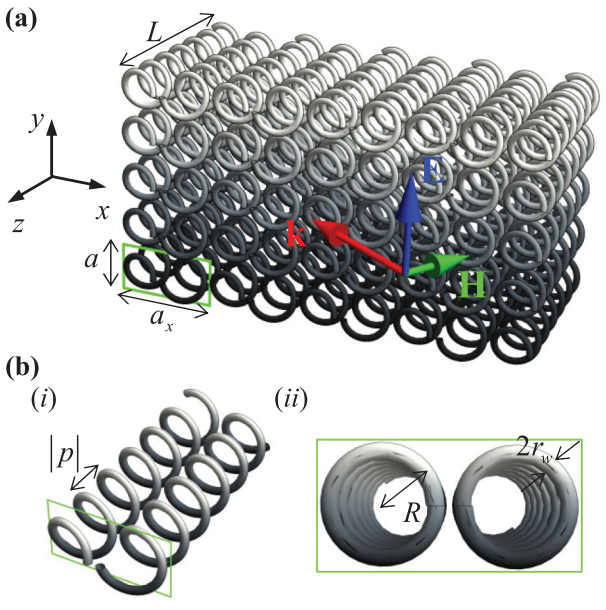

FIG. 1. (a) Geometry of the magnetic wire medium: a periodic array of helical-shaped metallic wires arranged in an orthorhombic lattice (period $a_x = 2a$ along the x direction, period a along the y direction, and period $|p|$ along the z direction). Each unit cell includes one right-handed helix and one left-handed helix. R is the radius of the helices and r_w is the radius of the wires. The helices stand in free-space. The plane of incidence is the xoz plane and the incident wave is TE-z polarized [$\mathbf{k} = (k_x, 0, k_z^{\text{inc}}), \mathbf{E} = E^{\text{inc}}\hat{\mathbf{u}}_y$]. (b) Unit cell of the metamaterial. (i) Perspective view and (ii) front view.

The electromagnetic response of the magnetic wire medium can be characterized using effective medium theory [31,32]. In general, the magnetic wire medium behaves as a spatially dispersive nonbianisotropic magnetic material that can be described by the following relative effective permeability and permittivity [31]:

$$\overline{\overline{\mu_r}} = \begin{pmatrix} 1 & 0 & 0 \\ 0 & 1 & 0 \\ 0 & 0 & \mu_{zz} \end{pmatrix}, \quad \mu_{zz} = \left(1 + \frac{A^2 k_0^2}{\frac{k_0^2}{\beta_{p1}^2} - \frac{k_z^2}{\alpha \beta_{p2}^2}} \right)^{-1},$$

$$\overline{\overline{\varepsilon_r}} = \begin{pmatrix} \varepsilon_t & 0 & 0 \\ 0 & \varepsilon_t & 0 \\ 0 & 0 & \varepsilon_{zz} \end{pmatrix},$$

$$\varepsilon_{zz} = 1 - \frac{1}{\frac{k_0^2}{\beta_{p1}^2} - \frac{k_z^2}{\beta_{p2}^2}} + \frac{A^2 k_0^2}{\left(1 + \frac{A^2 k_0^2}{\frac{k_0^2}{\beta_{p1}^2} - \frac{k_z^2}{\beta_{p2}^2}} \right) \left(\frac{k_0^2}{\beta_{p1}^2} - \frac{k_z^2}{\beta_{p2}^2} \right)^2}, \quad (1)$$

where $k_0 = \omega/c$, $A = \pi R^2/|p|$, β_{p1} and β_{p2} are parameters (with unities of m^{-1}) that only depend on the geometry of the material and whose definitions can be found in Ref. [32], and α is a correction factor intended to improve the accuracy of the analytical homogenization model. As detailed ahead, the correction factor is adjusted by hand by comparing the exact band structure of the metamaterial with the analytical result. In the above, $\varepsilon_t = \varepsilon_{xx} = \varepsilon_{yy} = 1 + [(\pi R)^2/(V_{\text{cell}} C_1)]$ is the effective permittivity in the xoy plane, $V_{\text{cell}} = a^2|p|$ is the volume of the unit cell, and C_1 is a geometrical parameter whose definition may be found in [32].

It should be noted that the dispersion of the effective medium parameters in Eq. (1) is rather different from that of the spiral medium studied in Ref. [25]. The reason is that the model of Ref. [25] treats each spiral as a lumped impedance and thus it is only valid for spirals with a small pitch and a small diameter. Our model does not have such limitations because the detailed microstructure of the helices is fully taken into consideration [32]. For completeness, it is also mentioned that the symmetry of the magnetic wire medium can be increased by arranging the helices in a checkerboard pattern (see also Ref. [28]). This alternative configuration would also eliminate the magnetoelectric coupling and would enforce at the same time a twofold rotational symmetry about the z axis. Such an increased symmetry may improve the validity of the continuous medium approximation, which treats the effective medium as isotropic in the xoy plane.

Next, the analysis is focused on the study of the propagation of TE-z polarized waves (electric field parallel to the xoy plane). The dispersion characteristic of the TE-z plane waves supported by the metamaterial is determined by [31]

$$k_0^2 \varepsilon_t - \frac{1}{\mu_{zz}} k_t^2 - k_z^2 = 0, \quad (2)$$

where $k_t^2 = k_x^2 + k_y^2$. It can be shown that the characteristic equation (2) reduces to a polynomial equation of second degree in the variables k_0^2 and k_z^2. Thus, the medium supports two independent plane wave modes with electric field in the xoy plane (TE-z plane waves). The emergence of an additional wave is a consequence of the spatially dispersive (or nonlocal)

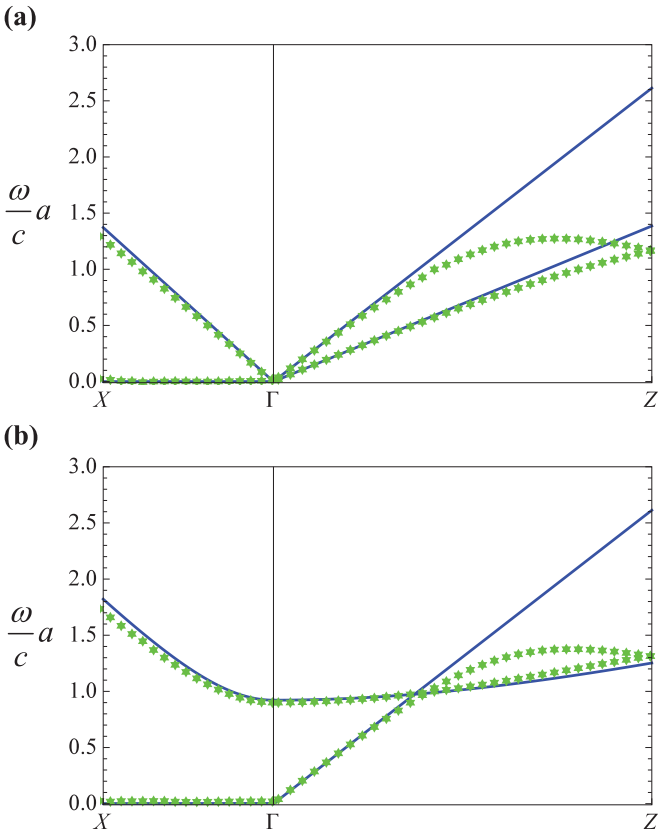

FIG. 2. Band structure for a magnetic wire medium with $R = 0.4a$, $r_w = 0.05a$, and $|p| = 0.9a$ (only the first four bands are shown). (a) TE-z modes. (b) TM-z modes. Solid lines: nonlocal homogenization results; star-shaped symbols: full-wave method of Ref. [33]. Γ, X, and Z are the highly symmetric points of the Brillouin zone.

response of the metamaterial [31,32]. In fact, this nonlocal response is manifest from Eq. (1), since the permeability depends not only on the frequency but also on the wave vector.

To validate the homogenization model, we calculated the dispersion characteristic of the Bloch waves supported by the metamaterial along the segments ΓX (propagation along the x direction) and ΓZ (propagation along the z direction) of the Brillouin zone (see Fig. 2). The relevant points are defined as $\Gamma = (0,0,0)$, $X = (\pi/a_x,0,0)$, and $Z = (0,0,\pi/|p|)$. Figure 2 shows the band structure of both the TE-z eigenwaves [Fig. 2(a)] and of the TM-z eigenmodes [Fig. 2(b)]. The band structure of the TE-z eigenwaves is calculated using the characteristic equation (2), whereas the band diagram of the TM-z eigenwaves is obtained from Eq. (7) of Ref. [31].

The dispersion curves predicted by the nonlocal homogenization model (solid lines) are compared with the full-wave method reported in Ref. [33] (star-shaped symbols). It is seen that the agreement between the results obtained with the two methods is very good, particularly for frequencies $\omega a/c < 1.0$. The disagreement observed at higher frequencies is due to the fact that the effective medium model is accurate only in the long wavelength limit [32]. The parameter α in Eq. (1) was tuned by hand to improve the agreement between the homogenization and the full-wave results for the TE eigenwaves case. For the particular geometry considered in this work ($R = 0.4a$, $r_w = 0.05a$, $|p| = 0.9a$), the correction factor is $\alpha = 0.51$. The remaining parameters used in the homogenization model are $C_1 \simeq 2.237/a$, $\beta_{p1} \simeq 1.075/a$, and $\beta_{p2} \simeq 3.794/a$.

Both calculation methods predict that the magnetic wire medium supports two low-frequency eigenwaves for each fixed polarization (TE-z or TM-z) [31]. Notably, the two TE-z eigenwaves have no low frequency cutoff, and hence the two TE waves can propagate with no decay for arbitrarily long wavelengths. This is a rather peculiar and unusual property, and it implies that the magnetic wire medium supports three *propagating* waves in the long wavelength limit, in contrast with standard Maxwellian media which only support two wave polarizations. This property seems to be a consequence of the fact that the unit cell of the metamaterial contains two infinitely long helices [34,35]. Note that even though the standard wire medium (formed by straight metallic wires) supports three eigenmodes [36,37], one of the eigenmodes has a low frequency cutoff. Hence, in this specific regard the physics of magnetic wire medium differs from that of the conventional wire medium.

To better understand the nature of the two TE modes, we show in Fig. 3 their isofrequency contours. Quite interestingly, one can see that the isofrequency contours associated with one of the modes are hyperbolic, whereas the contours associated with the other mode are elliptical. The two regimes (hyperbolic and elliptical) coexist in the same material for the same (TE) polarization and arbitrarily long wavelengths. This unveils the unique dual nature of the magnetic wire medium electromagnetic response.

The hyperbolic-type contours are nearly flat [Fig. 3(a)], so that k_z is nearly independent of k_t. This property is consistent with the microstructure of the metamaterial which suggests a strongly anisotropic response. A bit surprisingly, the isofrequency contours of the eigenmode with elliptical-type dispersion [Fig. 3(b)] are approximately circular. The dependence of the isofrequency contours of the two eigenmodes on the helix pitch is discussed in the Appendix.

Importantly, the isofrequency contours of Fig. 3(a) resemble those of the quasi-TEM mode supported by the standard wire medium in the infrared regime [20]. This suggests that the eigenmode with hyperbolic dispersion may enable a canalization regime analogous to that made possible by the quasi-TEM mode in the standard wire medium. Thus, the evanescent spatial spectrum of a TE-polarized near-field source placed in the vicinity of the metamaterial may be channeled through the metamaterial slab along the axial direction (z direction). As illustrated in Fig. 3(a), the energy inside the metamaterial slab always flows along a direction nearly parallel to the z direction (the Poynting vector is directed mostly along z), independent of the transverse wave number k_t.

To further validate the homogenization model, we depict in Fig. 4 the effective permeability along the z direction (μ_{zz}) as a function of k_z at a particular frequency of operation. The accuracy of the analytical result calculated from Eq. (1) (solid line) is checked against the numerical results obtained from the full-wave homogenization method proposed in [38]

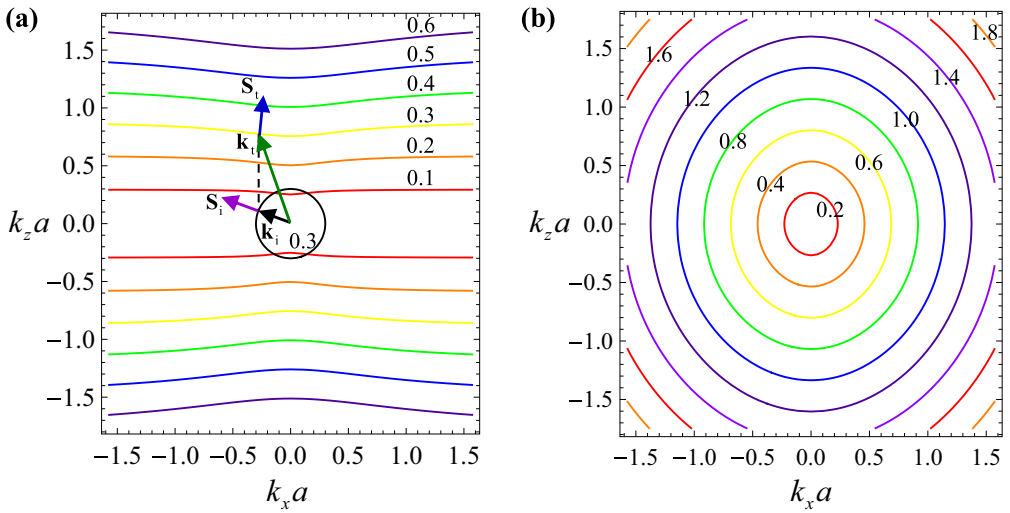

FIG. 3. Isofrequency contour of the two TE plane wave modes for propagation in the xoz plane with electric field perpendicular to this plane: (a) hyperbolic-type modes and (b) elliptical-type modes. The number insets specify the value of $\omega a/c$ associated with each curve. The geometrical parameters are as in Fig. 2. Panel (a) also depicts an isofrequency contour in the air region (black curve), and shows generic incident and transmitted wave vectors, as well as the corresponding Poynting vectors. The transmitted wave vector $\mathbf{k}_t$ (green arrow) is determined by the conservation of the tangential component of the wave vector k_x, whereas the Poynting vector $\mathbf{S}_t$ (blue arrow) is normal to the isofrequency curves and is oriented towards increasing frequencies.

(star-shaped symbols). As seen in Fig. 4, the results obtained using the two different methods concur very well. The range of the horizontal axis (k_z) in the plot is consistent with the isofrequency contour of the TE mode with hyperbolic dispersion at the same frequency (inset of Fig. 4). Note that Fig. 4 effectively represents the permeability seen by the TE modes with hyperbolic dispersion, which varies from mode to mode because of the nonlocal effects.

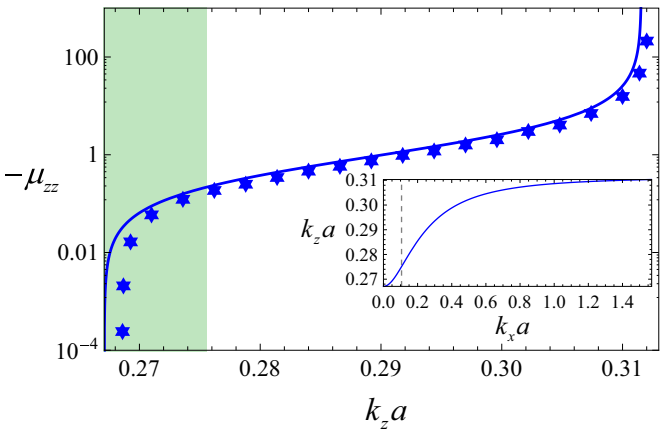

FIG. 4. Relative effective permeability μ_{zz} for a magnetic wire medium as a function of k_z with $R = 0.4a$, $r_w = 0.05a$, and $|p| = 0.9a$ at the normalized frequency $\omega a/c = 0.106$. Solid lines: analytical formula (1); star-shaped symbols: numerical results obtained using the full-wave homogenization approach reported in Ref. [38]. The range of k_z in the horizontal axis is coincident with that of the isofrequency contour of the TE eigenmode with hyperbolic-type dispersion at the same frequency (see the inset). The shaded (green) region in the main plot represents the range of k_z for which $k_x \leqslant k_0$ (i.e., the spatial spectrum that can be excited with a propagating incident plane wave at an air interface). The gray dashed line in the inset marks the limit $k_x = k_0$.

In particular, modes with a transverse wave vector such that $k_t \leqslant k_0$ ($k_t > k_0$) are mapped into (out of) the shaded (green) region of the main plot. It therefore follows that modes with a large transverse wave vector effectively experience a very negative effective permeability and an extreme anisotropy ratio $|\mu_{zz}| \gg 1$. These modes can be excited from the air region by an evanescent near field. On the other hand, waves with a small transverse wave vector ($k_t \ll k_0$) experience a near-zero permeability. Hence the eigenmodes with hyperbolic dispersion and $k_t \approx 0$ are essentially magnetoinductive waves [39]. These longitudinal-type modes occur when $\mu_{zz} = 0$ [40], and their properties were extensively studied in chains of magnetically coupled resonators [39–41].

To conclude this section, we note that it is crucial to have two helical-shaped wires with opposite handedness within the same unit cell to enable a near-field transport of TE-polarized waves. Indeed, it can be checked (not shown here) that for a metamaterial formed by helical-shaped wires with a fixed handedness (right-handed or left-handed helices), the electromagnetic mode that has a hyperbolic-type dispersion has an electric nature ($|\varepsilon_{zz}| \gg 1$, $|\mu_{zz}| \sim 1$, and $|\zeta_{zz}/\varepsilon_{zz}| \ll 1$, with ζ_{zz} being the effective parameter associated with the magnetoelectric coupling [32]). In our design, the chirality suppression creates an additional electromagnetic mode associated with a very large (and negative) magnetic permeability ($|\mu_{zz}| \gg 1$) (Fig. 4). This new electromagnetic mode results from the magnetic coupling between neighboring helices with opposite handedness, which enables a localized field distribution in each unit cell that is weakly radiative in the xoy plane so that for large k_t the energy is forced to flow along the z direction. Thus, similar to the standard wire medium lens, the magnetic wire medium may behave as a set of uncoupled "magnetic" waveguides.

III. TRANSMISSION PROPERTIES

Next, the scattering properties of the metamaterial slab (Fig. 1) are studied under plane wave incidence using the nonlocal homogenization model [Eq. (1)] and with full-wave simulations [42]. The metamaterial slab is assumed infinite and periodic along the x and y directions (with lattice period $2a$ and a, respectively), and finite along the z direction (with thickness L). The incident wave propagates in the xoz plane ($k_y = 0$) and the incoming electric field is polarized along the y direction (see Fig. 1). Thus, the electric field in the three regions of space can be written as follows (the x dependence and the time variation $e^{j\omega t}$ are suppressed):

$$\begin{aligned} E_y^{(1)} &= E_y^{\text{inc}}(e^{\gamma_0 z} + \rho e^{-\gamma_0 z}), \quad z > 0, \\ E_y^{(2)} &= A_1^+ e^{-jk_z^{(1)} z} + A_1^- e^{+jk_z^{(1)} z} + A_2^+ e^{-jk_z^{(2)} z} + A_2^- e^{+jk_z^{(2)} z}, \\ &\qquad -L < z < 0, \\ E_y^{(3)} &= E_y^{\text{inc}} \tau\, e^{\gamma_0 (z+L)}, \quad z < -L, \end{aligned} \tag{3}$$

where E_y^{inc} is the incident electric field, $\gamma_0 = \sqrt{k_x^2 - \omega^2 \varepsilon_0 \mu_0}$ is the free-space propagation constant, $k_x = \omega\sqrt{\varepsilon_0 \mu_0}\sin\theta_{\text{i}}$ (θ_{i} is the angle of incidence), and ρ and τ are the reflection and transmission coefficients, respectively. The propagation constants $k_z^{(1,2)}$ [calculated by solving Eq. (2) with respect to k_z] and the amplitudes $A_{1,2}^{\pm}$ are associated with the two TE modes (with elliptical and hyperbolic dispersions) that can be excited in the metamaterial slab. For each plane wave with electric field of the form $\mathbf{E} = E_0 e^{-j\mathbf{k}\cdot\mathbf{r}}\hat{\mathbf{u}}_y$, the corresponding magnetic field is given by

$$\mathbf{H} = \frac{E_0}{\eta_0 k_0}\left(-k_z \hat{\mathbf{u}}_x + \frac{k_x}{\mu_{zz}}\hat{\mathbf{u}}_z\right) e^{-j\mathbf{k}\cdot\mathbf{r}}. \tag{4}$$

To calculate the transmission and reflection coefficients, we impose that the tangential components of the electromagnetic fields (E_y and H_x) are continuous at the interfaces $x = 0$ and $x = -L$. Since there are two plane wave modes with the same polarization, these classical boundary conditions are insufficient to determine all the unknowns of the scattering problem [Eq. (3)]. To remove the extra degrees of freedom, the classical boundary conditions must be complemented with an additional boundary condition (ABC) at both interfaces. In analogy with the standard wire medium case [43–45], it is imposed that the normal component of the magnetic field (H_z) is continuous at the interfaces $x = 0$ and $x = -L$. This ABC is equivalent to ensure that the z component of the effective macroscopic magnetic current density [$\mathbf{J}_{\text{m}} = j\omega(\mathbf{B} - \mu_0\mathbf{H})$] vanishes at the interfaces, which is the magnetic counterpart of the usual wire medium case [43–45]. Indeed, the standard Maxwellian boundary conditions guarantee that B_z is always continuous, and hence the classical boundary conditions together with the condition that μH_z is continuous imply that $\mathbf{J}_{\text{m}} \cdot \hat{\mathbf{u}}_z = j\omega(B_z - \mu_0 H_z)$ is also continuous at the interface. Because $B_z - \mu_0 H_z$ is zero at the air side of the interface it follows that $\mathbf{J}_{\text{m}} \cdot \hat{\mathbf{u}}_z$ vanishes at the magnetic wire medium side of the interface, consistent with our claim. By imposing the ABC and the classical boundary conditions, we obtain a 6×6 linear system that can be numerically solved with respect to the unknowns.

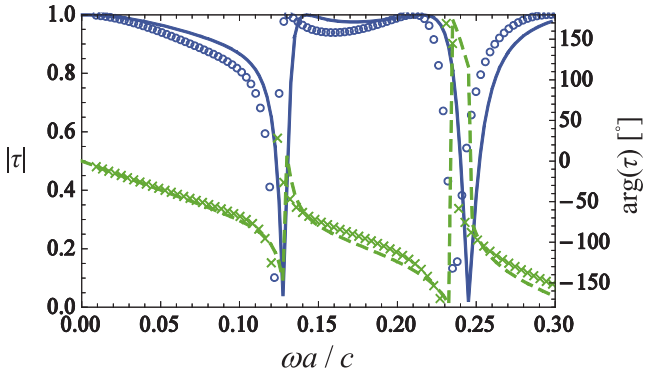

FIG. 5. Amplitude and phase of the transmission coefficient as a function of the normalized frequency, under plane wave incidence with $\theta_{\text{i}} = 45^\circ$. The geometrical parameters are $R = 0.4a$, $r_{\text{w}} = 0.05a$, $|p| = 0.9a$, and $L = 10a$. The solid curves (continuous lines: amplitude; dashed lines: phase) correspond to nonlocal homogenization results, whereas the discrete symbols (circles: amplitude; crosses: phase) correspond to full-wave results [42].

The amplitude and phase of the transmission coefficient for an incident plane wave with $\theta_{\text{i}} = 45^\circ$ is depicted in Fig. 5 as a function of the normalized frequency. It is seen that the results obtained with the nonlocal homogenization model and the proposed ABC (solid lines) agree well with the results obtained with the full-wave electromagnetic simulator CST Microwave Studio [42], demonstrating in this manner the validity of the proposed ABC.

In Fig. 6(a) the amplitude of the transmission coefficient is depicted as a function of the transverse wave vector k_x. The solid lines are associated with the nonlocal homogenization approach, whereas the dashed lines were obtained with CST Microwave Studio [42]. The thickness of the slab was tuned so that the Fabry-Perot resonance ($k_z^{(1)} L = \pi$) is satisfied around the normalized frequency $\omega a/c = 0.106$ [$k_z^{(1)} \approx (k_0\beta_{\text{p2}}/\beta_{\text{p1}})\sqrt{\alpha(1 + A^2\beta_{\text{p1}}^2)}$ is the propagation constant of the eigenwave with nearly flat dispersion], consistent with the usual canalization regime [17].

As seen in Fig. 6(a), the full-wave results (dashed lines) compare well with the analytical model (solid lines) for incident waves with $k_x c/\omega < 1$. In particular, both methods predict that for frequencies around the Fabry-Perot resonance the amplitude of the transmission coefficient is near unity for propagating waves ($k_x c/\omega \leqslant 1$). For evanescent waves the agreement deteriorates considerably, even though some qualitative features of the transmission characteristics are well reproduced by the analytical model, such as the enhancement of a significant part of the spectrum of the evanescent spatial harmonics ($1 < k_x c/\omega < 5$). Thus, these results suggest that somewhat analogous to the standard wire medium lens, which enables the transport of TM-z polarized waves [17], the considered magnetic wire medium lens may channel the TE-z polarized waves.

The imperfect agreement between the nonlocal homogenization results and the CST results may be attributed in part to resonant character of the Fabry-Perot condition, which makes the transmission coefficient of evanescent harmonics highly sensitive to variations of the structural parameters, and

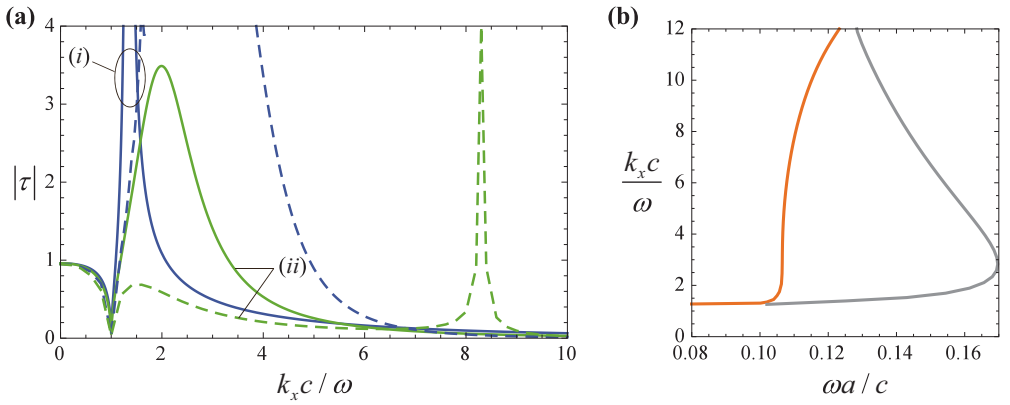

FIG. 6. (a) Amplitude of the transmission coefficient as a function of the normalized k_x for different frequencies of operation. The geometrical parameters are as in Fig. 5. (i) $\omega a/c = 0.106$ and (ii) $\omega a/c = 0.111$. Solid lines: nonlocal homogenization results [Eq. (3)]; dashed lines: full wave results [42]. (b) Propagation constant k_x of the two low-frequency guided modes supported by the metamaterial slab as a function of frequency, calculated with the eigenmode solver of CST Microwave Studio [42].

in part to the limitations of the effective medium model, which requires that $|k_x|a \ll 1$ and hence breaks down for evanescent waves [32]. In particular, the nonlocal homogenization model predicts that at $\omega a/c = 0.111$ the transmission coefficient does not exhibit a resonant behavior [see Fig. 6(a)(ii)], and thus the metamaterial slab should not support guided modes at this frequency. Differently, the full-wave simulations show that the metamaterial slab supports guided modes traveling along the x direction in a wide frequency range that includes $\omega a/c = 0.111$ [see Fig. 6(b)].

Even though for the canalization regime it would be desirable to have $|\tau| \approx 1$ for all spatial harmonics (including evanescent waves), it will be shown in the next section that the transfer function of the magnetic wire medium [Fig. 6(a)] can be used to transport the near field in an effective manner.

IV. MAGNETIC NEAR-FIELD IMAGING

In order to assess the subwavelength imaging potentials of the magnetic wire medium, next we consider scenarios wherein a material slab is illuminated by sources that radiate TE-z polarized waves. First, we use the nonlocal homogenization model to investigate the possibility of channeling the near field created by two line sources. In a later stage, the electromagnetic response of a finite width and height metamaterial slab illuminated by small magnetic loops is simulated using CST Microwave Studio [42].

To begin with, we consider that the metamaterial slab is illuminated by two infinitely extended y-oriented line sources separated by a subwavelength distance ($\Delta_s = 0.3\lambda_0$) and fed by electric currents in phase [Fig. 7(a)]. The two sources are placed at a distance $d_1 = a$ from the front interface. The electric field radiated by the line sources is of the form $E_y = [E_{y,0}/(4j)][H_0^{(2)}(k_0\rho_1) + H_0^{(2)}(k_0\rho_2)]$, where $E_{y,0}$ is some constant that depends on the electric current, ρ_1 and ρ_2 are the radial distances relative to the sources, and $H_0^{(2)}$ is the Hankel function of second kind and order zero. The fields radiated by the source can be decomposed into a spectrum of plane waves, i.e., the Hankel function can be represented as a Fourier integral of plane waves. Hence, considering that the line source is located at $z = d_1$, its electric field is of the form

$$E_y(x,z) = \frac{A}{\pi}\int_0^\infty \frac{1}{2\gamma_0} e^{-\gamma_0|z-d_1|}\cos(k_x x)dk_x. \tag{5}$$

The response of the system to this excitation can be obtained by superimposing the waves scattered by each plane wave in the decomposition (5). Thus, the electric field in the three regions of space can be written as follows:

$$\begin{aligned} E_y^{(1)}(x,z) &= \frac{A}{\pi}\int_0^\infty \frac{1}{2\gamma_0}[e^{-\gamma_0|z-d_1|} + \rho(\omega,k_x)e^{-\gamma_0(z+d_1)}] \\ &\quad \times \cos(k_x x)dk_x, \quad z > 0, \\ E_y^{(2)}(x,z) &= \frac{A}{\pi}\int_0^\infty \frac{1}{2\gamma_0} E_y^{(2)}(k_x,z)e^{-\gamma_0 d_1}\cos(k_x x)dk_x, \\ &\quad -L < z < 0, \\ E_y^{(3)}(x,z) &= \frac{A}{\pi}\int_0^\infty \frac{1}{2\gamma_0}\tau(\omega,k_x)e^{\gamma_0(z+L-d_1)}\cos(k_x x)dk_x, \\ &\quad z < -L. \end{aligned} \tag{6}$$

In the above, $E_y^{(2)}(k_x,z)$ is the electric field inside the slab ($-L < z < 0$) defined in Eq. (3), and $\rho(\omega,k_x)$ and $\tau(\omega,k_x)$ are the reflection and transmission coefficients obtained by solving the plane wave scattering problem [Eq. (3)]. Using the above equations we have calculated the electric field profile in all regions of space.

Figure 7(b)(i) shows a density plot of the squared electric field amplitude $|\mathbf{E}|^2$ in the xoz plane. In addition, to have a benchmark for this result, we also show the density plot of $|\mathbf{E}|^2$ when the helical-wire medium lens is removed [Fig. 7(b)(ii)], i.e., the radiation propagates only through the vacuum region. Figure 7(b)(i) clearly proves that the magnetic wire medium lens channels the radiation of the two line sources separated by a subwavelength distance, so that the radiated fields do not suffer a significant lateral spreading as when they propagate in free-space [Fig. 7(b)(ii)].

Figure 7(c) depicts the normalized squared electric field amplitude at the source and image planes, both in the presence and absence of the magnetic wire medium lens. It is seen that when the metamaterial lens is present, the two sources

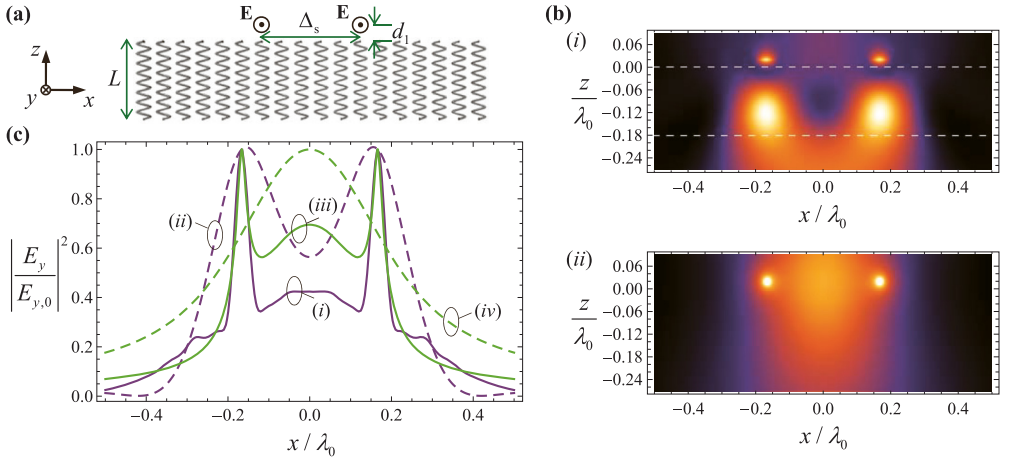

FIG. 7. (a) Geometry of the problem: two line sources fed by an electric current are separated by a distance Δ_s and placed at a distance d_1 above the magnetic wire medium slab. (b) Squared electric field amplitude $|\mathbf{E}|^2$. (i) Magnetic wire medium lens with the same geometrical parameters as in Fig. 5 and $\varepsilon_h = 1$, $\Delta_s = 0.3\lambda_0$, $d_1 = a$, and $\omega a/c = 0.1135$. The white dashed lines represent the interfaces of the lens. (ii) The same as in (i) but with the magnetic wire medium lens removed. (c) Amplitude of the normalized $|\mathbf{E}|^2$ at the source ($z = d_1/2$; solid lines) and image ($z = -L - d_1/2$; dashed lines) planes. (i) and (ii) are the results with the magnetic wire medium slab; (iii) and (iv) are the results without the magnetic wire medium slab.

are perfectly discernible from one another at the image plane [Fig. 7(c)(ii)], different from what happens when the lens is absent [Fig. 7(c)(iv)].

In order to verify the previous results based on homogenization theory, we have simulated the electromagnetic response of the metamaterial slab under similar conditions using the commercial electromagnetic simulator [42]. However, instead of using two electric line sources as the excitation, now we use small magnetic loops parallel to the interface plane. Moreover, we assume that the slab is finite along the x and y directions.

In a first scenario [Fig. 8(a)] we simulated the case wherein two small magnetic loops are separated by a subwavelength distance $\Delta_s = 0.3\lambda_0$ along the x direction and are placed at a distance $d_1 = a$ from the front interface of the metamaterial lens. The slab has dimensions $L_x = 46a$ and $L_y = 15a$ along the x and y directions, respectively. The results of the simulation at the frequency $f = 1.012$ GHz are presented in Fig. 8(b).

It is clear from Fig. 8(b) that the magnetic wire medium lens transports the radiation along the axial direction (z direction) without a significant lateral spreading. As a result, notwithstanding the subwavelength distance between the magnetic sources ($\Delta_s \approx 0.3\lambda_0$), the two loops are perfectly discernible at the image plane.

In order to estimate the bandwidth of operation and the resolution of this imaging device, we show in Fig. 8(c) the $|H_z|$ field profiles at the image plane for five different frequencies in the range 0.8–1.2 GHz. As one can see from Fig. 8(c), the two sources are resolved for frequencies in the interval 0.9–1.1 GHz. Therefore, the bandwidth of operation of the magnetic wire medium lens is about 18%, which is comparable to that of the standard wire medium lens [16] and to the best of our knowledge is nearly an order of magnitude better than the bandwidth provided by a Swiss rolls-based lens [4,5]. The half-power beamwidth (HPBW) at the image plane for $f = 1.0$ GHz [Fig. 8(c)(iii)] is about $\Delta_s = 0.075\lambda_0 \simeq 4.45a$. This resolution is about twice the largest lattice period ($\Delta_s \approx 2a_x$) similar to the typical resolution provided by standard wire medium lenses formed by straight wires [16]. This result is explained by the fact that non-neighboring helices are weakly coupled for $k_{||} \gg k_0$ because $|\mu_{zz}| \gg 1$, and hence they provide a pixel by pixel near-field transport. This behavior is different from that characteristic of the systems studied in Ref. [46], wherein the significant mutual interaction between the different resonators limits the resolution to several lattice constants.

To fully evaluate the resolution capabilities of the metamaterial lens along the y direction, we investigated the case where the sources are distributed both along the x and y directions. Specifically, we consider a scenario wherein eight small magnetic loops are disposed in the form of a ring very close to each other at a distance $d_1 = a$ away from the slab front interface [see Fig. 9(a)]. The distance between adjacent loops is $\Delta_s = 0.08\lambda_0$. In this case, the slab has dimensions $L_x = 46a$ and $L_y = 27a$ along the x and y directions, respectively.

Figure 9(b) depicts the density plots of the magnetic field amplitude $|H_z|$ for $f = 1.012$ GHz at the source and image planes. These results clearly prove that the magnetic wire medium lens resolves the sources separated by deeply subwavelength distances ($\Delta_s = 0.08\lambda_0 \sim 2a_x$). Moreover, even though the microstructure of the lens is different along the two main axes (see Fig. 1) the metamaterial lens can discriminate objects disposed along either the x or y directions.

V. CONCLUSION

In this work we investigated the possibility of near-field imaging using a racemic array of helical-shaped metallic wires. Rather surprisingly, it was shown that two propagating TE-polarized eigenwaves coexist in the magnetic wire medium in the quasistatic limit. One of the modes has an elliptical-type dispersion, whereas the other mode has a hyperbolic (nearly flat) dispersion with respect to the transverse wave vector. The latter eigenmode enables a canalization regime for

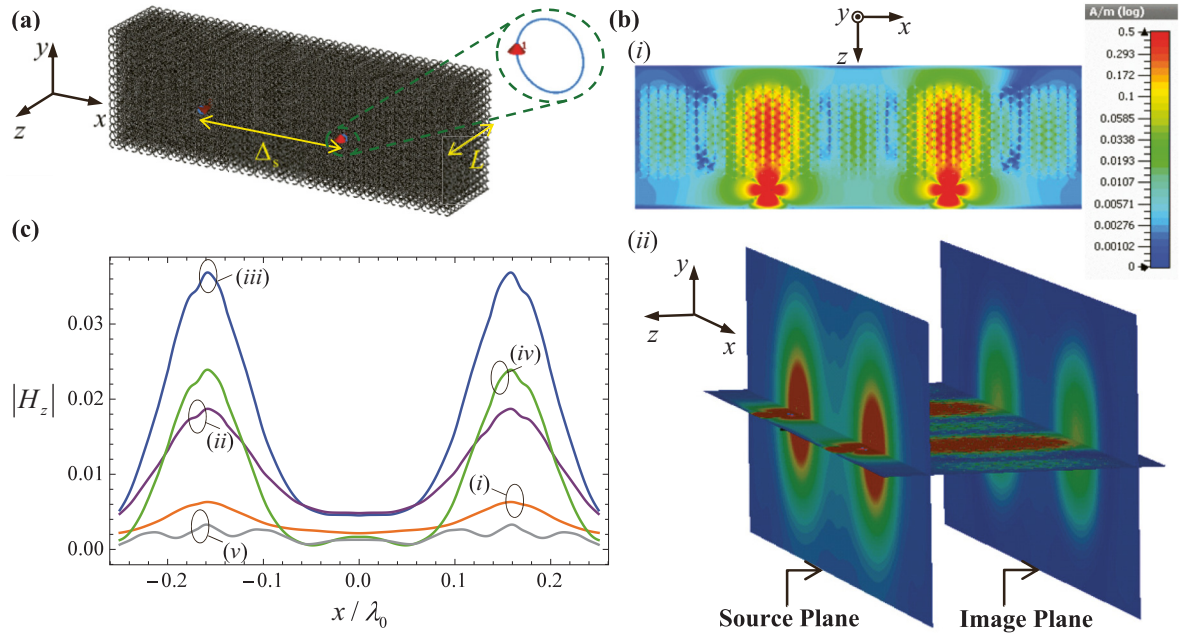

FIG. 8. (a) Geometry of the finite-sized magnetic wire medium lens: two magnetic loops are separated by a distance $\Delta_s = 8.89a_x \approx 0.3\lambda_0$ and placed at a distance $a = 5\,\text{mm}$ above from the input interface of the lens. (b) Amplitude of the magnetic field $|\mathbf{H}|$ for a magnetic wire medium lens with the same geometrical parameters as in Fig. 5 and $\varepsilon_h = 1$, $d_1 = a$, $\Delta_s = 0.3\lambda_0$, and $f = 1.012\,\text{GHz}$, obtained using CST Microwave Studio [42]. (i) Top view and (ii) perspective view. (c) Amplitude of $|\mathbf{H}|$ at the image plane ($z = -L - a/2$) for different frequencies of operation. (i) $f = 0.8\,\text{GHz}$, (ii) $f = 0.9\,\text{GHz}$, (iii) $f = 1.0\,\text{GHz}$, (iv) $f = 1.1\,\text{GHz}$, and (v) $f = 1.2\,\text{GHz}$.

TE-polarized waves, and hence, in this regard, the racemic helical-shaped wire medium behaves as a magnetic analog of the conventional wire medium formed by straight metallic wires [15–17,20]. In particular, it was demonstrated with full-wave simulations that the magnetic wire medium lens enables the transport of the subwavelength details of TE-z polarized sources, similar to what is achieved with the standard wire medium for TM-polarized waves. Our findings may be useful for the development of novel microwave and terahertz imaging devices, and may also have applications in magnetic resonance imaging.

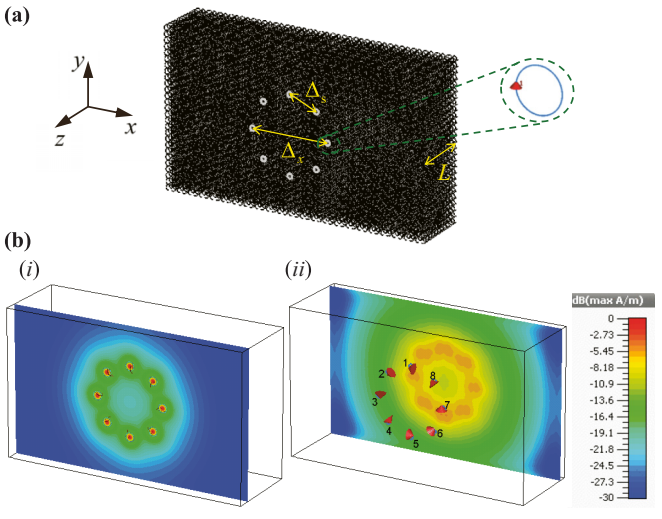

FIG. 9. (a) Geometry of the finite-sized magnetic wire medium lens: a ring of eight magnetic loops separated by a distance $\Delta_s = 0.08\lambda_0$ are placed at a distance $a = 5\,\text{mm}$ from the input interface of the lens. (b) Amplitude of the magnetic field $|\mathbf{H}|$ for a magnetic wire medium lens with the same geometrical parameters as in Fig. 5 and $\varepsilon_h = 1$, $d_1 = a$, $\Delta_s = 0.08\lambda_0$, $\Delta_x = 0.2\lambda_0$, and $f = 1.012\,\text{GHz}$, obtained with CST Microwave Studio [42]. (i) Source plane ($z = a/2$) and (ii) image plane ($z = -L - a/2$).

ACKNOWLEDGMENTS

This work was funded by Fundação para a Ciência e a Tecnologia under projects PTDC/EEI-TEL/2764/2012 and PTDC/EEI-TEL/4543/2014. T. A. Morgado acknowledges financial support by Fundação para a Ciência e a Tecnologia (FCT/POPH) and the cofinancing of Fundo Social Europeu under the Post-Doctoral fellowship SFRH/BPD/84467/2012.

APPENDIX: EFFECT OF THE HELIX PITCH ON THE METAMATERIAL CHANNELING PROPERTIES

In this Appendix we discuss the effect of the helix pitch p on the isofrequency contours of the eigenmodes and on the transmission properties of the metamaterial lens.

Figure 10 depicts the isofrequency contours of the two TE-z eigenmodes supported by the magnetic uniaxial wire medium for three different values of the helix pitch: $|p| = 0.5a$, $|p| = 0.9a$, and $|p| = 1.3a$. The results were obtained with the analytical model. As seen in Fig. 10(a), as the helix pitch p is increased, the isofrequency contour of the hyperbolic-type mode becomes more and more flat. On the other hand, the isofrequency contour of the elliptical-type mode is increasingly circular as the helix pitch is increased.

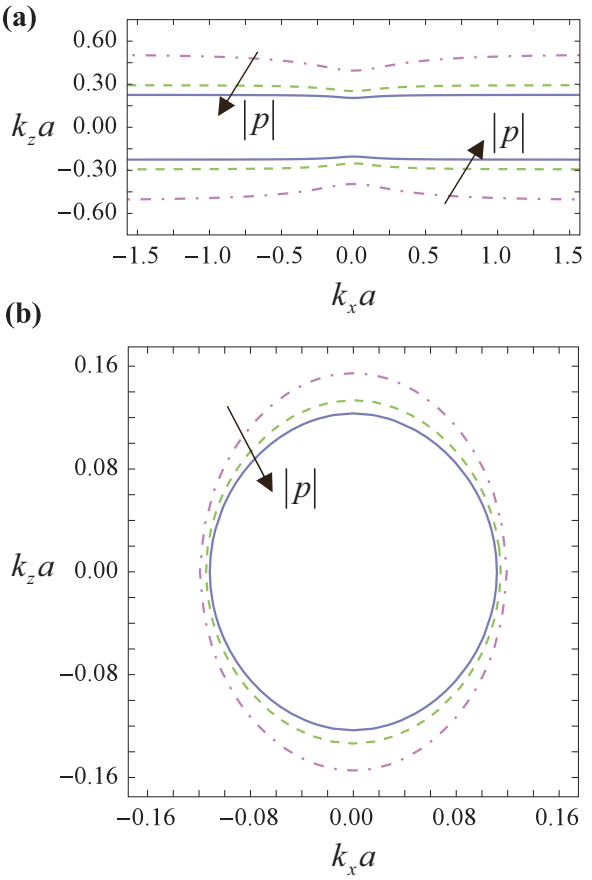

FIG. 10. Influence of the helix pitch on the isofrequency contours of the (a) hyperbolic-type and (b) elliptical-type eigenmodes for $R = 0.4a$, $r_w = 0.05a$, and $\omega a/c = 0.1$. Dot-dashed purple lines: $|p| = 0.5a$ and $\alpha = 0.35$. Dashed green lines: $|p| = 0.9a$ and $\alpha = 0.51$. Solid blue lines: $|p| = 1.3a$ and $\alpha = 0.64$.

Thus, it follows that it is advantageous to have a large helix pitch to have flat isofrequency surfaces.

However, one should keep in mind that both the hyperbolic- and the elliptical-type modes can be excited in the magnetic wire medium because both of them are propagating waves. Hence, in practice the quality of the imaging by a magnetic wire medium slab is determined not only by the flatness of the isofrequency surface of the hyperbolic mode, but also by how well the hyperbolic mode can be excited in the near-field region. Our numerical simulations indicate that for values of p comparable to or larger than $2a$ the hyperbolic mode is difficult to excite and hence the quality of the near-field

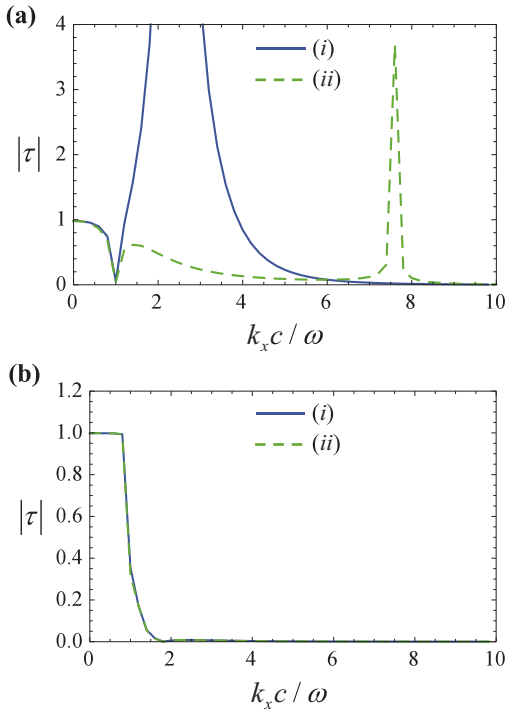

FIG. 11. Amplitude of the transmission coefficient as a function of the normalized k_x for different frequencies of operation and for a configuration with $R = 0.4a$ and $r_w = 0.05a$, calculated with the full-wave electromagnetic simulator [42] for (i) $\omega a/c = 0.098$, (ii) $\omega a/c = 0.1$. (a) $|p| = 1.5a$ and $L = 15.68a$. (b) $|p| = 2.0a$ and $L = 25.13a$.

imaging is poor. This is illustrated in Fig. 11, which shows the transmission coefficient as a function of the transverse wave vector for two different values of the helix pitch. The simulations were done using CST Microwave Studio [42] and the thickness of the magnetic wire medium slab was tuned in each case so that the hyperbolic-type mode experiences a Fabry-Perot resonance for normal incidence at $\omega a/c \sim 0.1$. As seen, the response for $|p| = 1.5a$ is qualitatively similar to that of Fig. 6(a)(i), whereas for $|p| = 2a$ the imaging properties are rather poor and the evanescent waves are not transported across the slab. These results suggest that having a small pitch favors the near-field coupling to the hyperbolic-type modes but deteriorates the flatness of the isofrequency contours. We found that $|p| = 0.9a$ (the value used in the examples of the main text) is a good compromise between these two conflicting objectives.

[1] E. Abbe, Arch. Mikroskop. Anat. **9**, 413 (1873).
[2] L. Rayleigh, Philos. Mag. **8**, 261 (1879).
[3] J. B. Pendry, Phys. Rev. Lett. **85**, 3966 (2000).
[4] M. C. K. Wiltshire, J. V. Hajnal, J. B. Pendry, D. J. Edwards, and C. J. Stevens, Opt. Express **11**, 709 (2003).
[5] M. C. K. Wiltshire, J. B. Pendry, W. Williams, and J. V. Hajnal, J. Phys. Condens. Matter **19**, 456216 (2007).
[6] N. Fang, H. Lee, C. Sun, and X. Zhang, Science **308**, 534 (2005).
[7] M. J. Freire and R. Marqués, Appl. Phys. Lett. **86**, 182505 (2005).
[8] M. J. Freire, R. Marques, and L. Jelinek, Appl. Phys. Lett. **93**, 231108 (2008).
[9] Z. Jacob, L. V. Alekseyev, and E. Narimanov, Opt. Express **14**, 8247 (2006).
[10] A. Salandrino and N. Engheta, Phys. Rev. B **74**, 075103 (2006).

[11] I. I. Smolyaninov, Y. J. Hung, and C. C. Davis, Science **315**, 1699 (2007).
[12] Z. Liu, H. Lee, Y. Xiong, C. Sun, and X. Zhang, Science **315**, 1686 (2007).
[13] R. Merlin, Science **317**, 927 (2007).
[14] A. Grbic, L. Jiang, and R. Merlin, Science **320**, 511 (2008).
[15] P. A. Belov, C. R. Simovski, and P. Ikonen, Phys. Rev. B **71**, 193105 (2005).
[16] P. A. Belov, Y. Hao, and S. Sudhakaran, Phys. Rev. B **73**, 033108 (2006).
[17] P. A. Belov and M. G. Silveirinha, Phys. Rev. E **73**, 056607 (2006).
[18] P. A. Belov, Y. Zhao, S. Sudhakaran, A. Alomainy, and Y. Hao, Appl. Phys. Lett. **89**, 262109 (2006).
[19] P. A. Belov, Y. Zhao, S. Tse, P. Ikonen, M. G. Silveirinha, C. R. Simovski, S. Tretyakov, Y. Hao, and C. Parini, Phys. Rev. B **77**, 193108 (2008).
[20] M. G. Silveirinha, P. A. Belov, and C. R. Simovski, Phys. Rev. B **75**, 035108 (2007).
[21] C. Luo, S. G. Johnson, J. D. Joannopoulos, and J. B. Pendry, Phys. Rev. B **68**, 045115 (2003).
[22] T. A. Morgado and M. G. Silveirinha, New J. Phys. **11**, 083023 (2009).
[23] T. A. Morgado, J. S. Marcos, M. G. Silveirinha, and S. I. Maslovski, Appl. Phys. Lett. **97**, 144102 (2010).
[24] C. Navau, J. Prat-Camps, O. Romero-Isart, J. I. Cirac, and A. Sanchez, Phys. Rev. Lett. **112**, 253901 (2014).
[25] P. A. Belov, C. R. Simovski, and S. A. Tretyakov, Phys. Rev. E **67**, 056622 (2003).
[26] J. K. Gansel, M. Thiel, M. S. Rill, M. Decker, K. Bade, V. Saile, G. von Freymann, S. Linden, and M. Wegener, Science **325**, 1513 (2009).
[27] C. Wu, H. Li, X. Yu, F. Li, H. Chen, and C. T. Chan, Phys. Rev. Lett. **107**, 177401 (2011).
[28] A. N. Lagarkov, V. N. Semenenko, V. A. Chistyaev, D. E. Ryabov, S. A. Tretyakov, and C. R. Simovski, Electromagnetics **17**, 213 (1997).
[29] A. Demetriadou, S. S. Oh, S. Wuestner, and O. Hess, New J. Phys. **14**, 083032 (2012).
[30] S. S. Oh, A. Demetriadou, S. Wuestner, and O. Hess, Adv. Mater. **25**, 612 (2013).
[31] T. A. Morgado, S. I. Maslovski, and M. G. Silveirinha, New J. Phys. **14**, 063002 (2012).
[32] M. G. Silveirinha, IEEE Trans. Antennas Propag. **56**, 390 (2008).
[33] M. G. Silveirinha and C. A. Fernandes, IEEE Trans. Microwave Theory Tech. **52**, 889 (2004).
[34] J. Shin, J.-T. Shen, and S. Fan, Phys. Rev. B **76**, 113101 (2007).
[35] G. W. Hanson, E. Forati, and M. G. Silveirinha, IEEE Trans. Antennas Propag. **60**, 4219 (2012).
[36] P. A. Belov, R. Marqués, S. I. Maslovski, I. S. Nefedov, M. G. Silveirinha, C. R. Simovski, and S. A. Tretyakov, Phys. Rev. B **67**, 113103 (2003).
[37] M. G. Silveirinha, Phys. Rev. E **73**, 046612 (2006).
[38] M. G. Silveirinha, Phys. Rev. B **75**, 115104 (2007).
[39] E. Shamonina, V. A. Kalinin, K. H. Ringhofer, and L. Solymar, J. Appl. Phys. **92**, 6252 (2002).
[40] J. D. Baena, L. Jelinek, R. Marqués, and M. Silveirinha, Phys. Rev. A **78**, 013842 (2008).
[41] P. A. Belov and C. R. Simovski, Phys. Rev. E **72**, 026615 (2005).
[42] CST Microwave Studio 2014, CST GmbH, http://www.cst.com.
[43] M. G. Silveirinha, IEEE Trans. Antennas Propag. **54**, 1766 (2006).
[44] M. G. Silveirinha, C. A. Fernandes, and J. R. Costa, New J. Phys. **10**, 053011 (2008).
[45] M. G. Silveirinha, New J. Phys. **11**, 113016 (2009).
[46] M. Lapine, L. Jelinek, M. J. Freire, and R. Marqués, Phys. Rev. B **82**, 165124 (2010).